Journal of Power Sources 240 (2013) 759–765

Contents lists available at SciVerse ScienceDirect

Journal of Power Sources

journal homepage: www.elsevier.com/locate/jpowsour

Lattice structure, sintering behavior and electrochemical performance of $La_{1.7}Ca_{0.3}Ni_{1-x}Cu_xO_{4+\delta}$ as cathode material for intermediate-temperature solid oxide fuel cell

Yongna Shen [a], Hailei Zhao [a,b,*], Konrad Świerczek [c], Zhihong Du [a], Zhixiang Xie [a]

[a] School of Materials Science and Engineering, University of Science and Technology Beijing, Beijing 100083, China
[b] Beijing Key Lab of New Energy Materials and Technologies, Beijing 100083, China
[c] Department of Hydrogen Energy, Faculty of Energy and Fuels, AGH University of Science and Technology, al. A. Mickiewicza 30, 30-059 Krakow, Poland

HIGHLIGHTS

- Cu-doping significantly enhances the sintering activity of the material.
- The electronic conductivity increases with the content of Cu.
- Cu-doping improves the electrochemical performance remarkably.

ARTICLE INFO

Article history:
Received 22 March 2013
Received in revised form
6 May 2013
Accepted 8 May 2013
Available online 16 May 2013

Keywords:
Lanthanum nickelate
Electronic conductivity
Polarization resistance
Cell performance

ABSTRACT

Cu-doped $La_{1.7}Ca_{0.3}NiO_{4+\delta}$ has been synthesized and evaluated as potential intermediate-temperature solid oxide fuel cell cathode materials. The effects of Cu substitution for Ni on lattice structure, sinterability, electrical and electrochemical properties of $La_{1.7}Ca_{0.3}NiO_{4+\delta}$ are investigated. Cu-doping significantly enhances the sintering activity of $La_{1.7}Ca_{0.3}Ni_{1-x}Cu_xO_{4+\delta}$. With increasing content of Cu, both the electronic conductivities and electrochemical performance remarkably increase, leading to an attractive cell performance. The increased conductivity may be related with the elongated $Ni(Cu)O_6$ octahedron in perovskite layers while the decreased polarization resistance mainly correlates with the improved oxygen transport property induced by replacement of Ni by Cu. Single cell test suggests that $La_{1.7}Ca_{0.3}Ni_{1-x}Cu_xO_{4+\delta}$ is a promising candidate for solid oxide fuel cell cathode.

© 2013 Elsevier B.V. All rights reserved.

1. Introduction

Recent years, many efforts have been devoted to identifying suitable cathode materials for solid oxide fuel cells (SOFCs) working at intermediate temperature. Mixed ionic–electronic conductors (MIEC) appear to be promising candidates due to the improvement of the kinetic of cathode reaction by extending the triple phase boundary to the entire cathode surface [1–4]. As a group of MIEC, La_2NiO_4-based oxides with K_2NiF_4 structure have been one of focuses of interest [5–9]. They not only exhibit high oxygen surface exchange and bulk diffusion coefficients comparable to that of $La_{1-x}Sr_xCo_{1-y}Fe_yO_{3-\delta}$, but also present moderate thermal expansion coefficient (TEC) compatible with common electrolyte such as YSZ, $Ce_{1.9}Gd_{0.1}O_{2-\delta}$ and $La_{0.8}Sr_{0.2}Ga_{0.83}Mg_{0.17}O_{3-\delta}$ (LSGM) [10–14]. The crystal structure of $La_2NiO_{4+\delta}$ is formed by stacking alternate $LaNiO_3$ perovskite layers and LaO rocksalt layers along the *c* direction and can accommodate a wide range of excess oxygen ($0.0 < \delta < 0.25$) in the rocksalt layers as interstitial defects, which are charge-compensated by the formation of electron holes on nickel cations. Due to mismatch between the La–O and Ni–O bonds, the rocksalt layers are compressed while the perovskite layers are stretched. The structural strain resulting can be minimized by either rotation of NiO_6 octahedron along the [110] direction of the ideal tetragonal I4/mmm structure or insertion of extra oxygen in rocksalt layers [15–17].

For practical application as a cathode, there are still some problems with $La_2NiO_{4+\delta}$. One of them encountered is the lack of

* Corresponding author. School of Materials Science and Engineering, University of Science and Technology Beijing, Beijing 100083, China. Tel./fax: +86 10 82376837.
E-mail addresses: hlzhao@ustb.edu.cn, hlzhao66@gmail.com (H. Zhao).

0378-7753/$ – see front matter © 2013 Elsevier B.V. All rights reserved.
http://dx.doi.org/10.1016/j.jpowsour.2013.05.025

sufficient electronic conductivity [18]. Because $La_2NiO_{4+\delta}$ is a p-type conductor, appropriate acceptor doping on A-site could improve the electronic conductivity by generating extra electron holes for charge compensation [19]. Alkaline-earths strontium and calcium, with similar ionic radii ($rCa^{2+} = 1.18$ Å and $rSr^{2+} = 1.31$ Å) and lower valence with respect to lanthanum ($rLa^{3+} = 1.216$ Å), have been identified to be suitable A-site doping elements [18,20–23]. However, the substitution La by Sr lowers the ionic conductivity of $La_2NiO_{4+\delta}$, due to the reduction of oxygen interstitials [14,24]. Although doping with Ca will also decrease the content of oxygen interstitials, $La_{2-x}Ca_xNiO_{4+\delta}$ has more excess oxygen than $La_{2-x}Sr_xNiO_{4+\delta}$ in order to release the enhanced tensile stress induced by the smaller radius of Ca^{2+} compared to Sr^{2+} [25]. Consequently, a better oxygen transport property is expected for $La_{2-x}Ca_xNiO_{4+\delta}$, since oxygen transport in $La_2NiO_{4+\delta}$ occurs mainly via the diffusion of oxygen interstitial in rocksalt layers [14,26]. Our previous work demonstrated that $La_{2-x}Ca_xNiO_{4+\delta}$ exhibits a higher ionic conductivity than the non-doped sample [22].

However, the substitution of La by Ca decreases the sinterability of $La_{2-x}Ca_xNiO_{4+\delta}$. The sintering activity is an important factor that can affect the contact between cathode and electrolyte and among the cathode particles, and further influence the oxygen ion transport across these interfaces [27,28]. Although increasing temperature can trigger the sintering activity of cathode materials, the high preparation temperature may cause chemical reaction between cathode and electrolyte. La_2CuO_4, with a same structure, has a lower melting point of about 1050 ± 10 °C [29] and is chemical compatible with LSGM [30], therefore, doping $La_{1.7}Ca_{0.3}NiO_{4+\delta}$ with Cu may be able to increase the sintering activity without compromising the chemical stability of electrode as it doping in La_2NiO_4 [13,31]. What is more, due to Jahn–Teller effect, Cu-doping always causes a shortened Ni(Cu)–O (equatorial) bond in $Ni(Cu)O_6$ octahedron, which can mitigate the rotation of $Ni(Cu)O_6$ octahedral and thus lead to a relaxation of the orthorhombic distortion of the microstructure [32]. This change may have a positive influence on the mass transport properties of $La_{2-x}Ca_xNiO_{4+\delta}$. In this study, Cu is selected as dopant to substitute partial Ni of $La_{1.7}Ca_{0.3}NiO_{4+\delta}$ with the aim of improving the sinterability and the electrode performance. The $La_{1.7}Ca_{0.3}Ni_{1-x}Cu_xO_{4+\delta}$ are prepared and the effects of Cu on the crystal structure, sintering behavior, and electrical and electrochemical properties of $La_{1.7}Ca_{0.3}Ni_{1-x}Cu_xO_{4+\delta}$ are investigated.

2. Experimental

2.1. Sample preparation

$La_{1.7}Ca_{0.3}Ni_{1-x}Cu_xO_{4+\delta}$ (LCNC, $x = 0.1, 0.2, 0.3$) powders were synthesized via citric–nitric method using analytical grade La_2O_3, $Ca(NO_3)_2{\cdot}4H_2O$, $Ni(NO_3)_2{\cdot}6H_2O$ and $Cu(NO_3)_2{\cdot}3H_2O$ as starting materials. The La_2O_3 was annealed at 1000 °C for 8 h before use to remove the possibly adsorbed water and carbon dioxide. Stoichiometric amounts of La_2O_3 and nitrate salts were dissolved into dilute nitric acid under magnetic stirring. Citric acid was then added to the mixture in molar ratio of 1:1.1 with regard to total metallic ions. The resulting solution was heated in a water bath at 80 °C to form a viscous gel, which was further heated on a hot plate for self-combustion, yielding a foam-like precursor. After pulverized with an agate mortar, the precursors were calcined at 750 °C for 6 h to get desired materials. Bars of 40 × 7 × 3 mm^3 of each composition were uniaxially pressed using polyethylene glycol as a binder at ca. 115 MPa and then sintered at 1000–1250 °C for 6 h to get dense samples for electrical conductivity measurement.

The electrolyte used in the experiments, $La_{0.8}Sr_{0.2}Ga_{0.83}Mg_{0.17}O_{3-\delta}$ (LSGM), was prepared by a combined EDTA–citrate sol–gel process. Metallic gallium was dissolved into HNO_3 at 80 °C before mixing with the solutions of $La(NO_3)_3$, $Sr(NO_3)_2$ and $Mg(NO_3)_2$. Citric acid and EDTA were added as chelating agent in a molar ratio of 1.5:1:1 with regard to the total metallic ions. After adjusting the pH to ~8 with ammonium, the mixture was heated till a gel was formed. The gel was first pre-fired at 250 °C and then calcined at 1100 °C for 10 h. Dense LSGM pellets were obtained by uniaxially pressing the powder under ca. 115 MPa and sintering at 1450 °C in air for 10 h.

Cells were fabricated using screen-printing technique. Suitable inks were prepared by mixing corresponding electrode powders with terpineol solution of 10 wt% ethylic cellulose in a mass ratio of 6:4 with agate mortar. For symmetrical cells, LCNC cathode inks were screen-printed on both sides of LSGM electrolyte in symmetrical configuration and sintered at 850–1000 °C for 2 h to form a porous electrode adhered well on the electrolyte. For electrolyte-supported cells, NiO–$Ce_{0.9}Gd_{0.1}O_{2-\delta}$ (GDC) in weight ratio of 6:4 was used as anode and $Ce_{0.6}La_{0.4}O_{2-\delta}$ (LDC) was used as a buffer layer to prevent the reaction between Ni and LSGM electrolyte. LDC slurry was first deposited on one side of LSGM electrolyte, followed by sintering at 1400 °C for 4 h. Anode inks were subsequently painted on LDC layer and fired at 1300 °C for 2 h prior to the application of the cathode ink. After printing the cathode ink on the other side of LSGM, the cell was fired at 950 and 850 °C for $x = 0.0$ and 0.3 for 4 h. Pt paste was used as current collection while Ag wires as lead wire for both electrodes.

2.2. Characterization

Phase purity of LCNC and chemical compatibility of LCNC with LSGM were examined by X-Ray diffraction (XRD) in a Rigaku D/max-A X-ray diffractometer with Cu-$K_{\alpha 1}$ radiation ($\lambda = 1.5406$ Å). To examine the chemical compatibility, the mixture of LCNC and LSGM in 1:1 mass ratio was pressed into pellets and sintered at different temperatures for 4 h. The sintered samples were crushed and then subjected to XRD examination. Rietveld refinements were performed for the compositions $La_{1.7}Ca_{0.3}Ni_{1-x}Cu_xO_{4+\delta}$ with $x = 0$ and 0.3 employing FULLPROF program. Data for Rietveld analysis were collected using PANalytical X'Pert Pro diffractometer (CuK_α, $\lambda_1 = 1.5406$ Å and $\lambda_2 = 1.54439$ Å) over a 2θ range of 10–130° with steps size of 0.02° and a counting time of 1 s per step. Bulk density of sintered bars was measured by Archimedes' method using distilled water as medium. Scanning electron microscopy (SEM, LEO-1450) was used to observe the microstructure of dense ceramics and porous electrodes. The total electrical conductivities were tested by four-terminal dc method over the temperature range of 150–800 °C in static air.

Solartron 1260 Frequency Response Analyzer combined with a Solartron 1287 potentiate was used to record the electrochemical impedance spectra (EIS) and current–voltage (I–V) curves. The ac impedance data were collected in the frequency region from 10^6 to 0.1 Hz with a signal amplitude of 5 mV. Area specific resistances (ASR) of symmetrical cells were measured in static air. For single cell, cells were sealed on an alumina tube with commercially available cement (Aremco Products. Inc., Ceramabond 552-VFG). The anode side was fed with humidified hydrogen (3% H_2O) at a flow rate of 50 ml min^{-1} while the cathode side worked in static air atmosphere.

3. Results and discussions

3.1. XRD

Fig. 1 shows the XRD patterns of LSGM, LCNC and LCNC–LSGM composites. The LCNC powders are calcined at 950 and 850 °C for compositions with $x = 0.1$ and 0.3, respectively, which are also the fabrication temperatures of corresponding cathode. The LCNC–

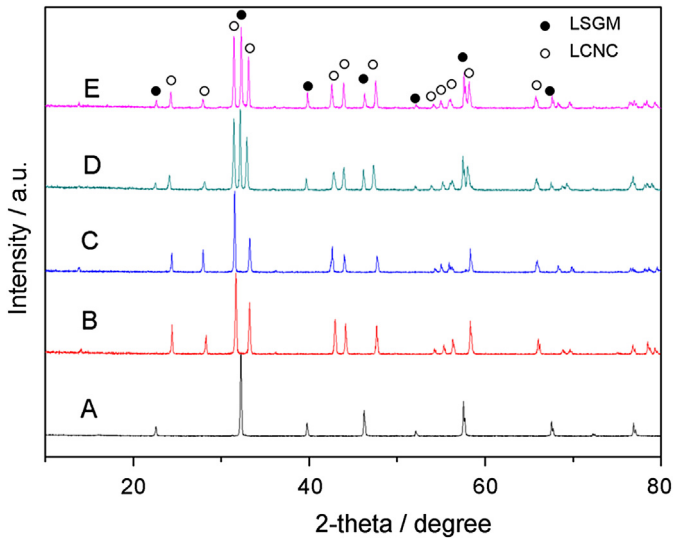

Fig. 1. XRD patterns of (A) LSGM; (B) $La_{1.7}Ca_{0.3}Ni_{0.9}Cu_{0.1}O_{4+\delta}$; (C) $La_{1.7}Ca_{0.3}Ni_{0.7}Cu_{0.3}O_{4+\delta}$; (D) $La_{1.7}Ca_{0.3}Ni_{0.9}Cu_{0.1}O_{4+\delta}$–LSGM mixture and (E) $La_{1.7}Ca_{0.3}Ni_{0.7}Cu_{0.3}O_{4+\delta}$–LSGM mixture.

LSGM composites are calcined at 1100 and 1000 °C for samples with $x = 0.1$ and 0.3, respectively. Each composition of LCNC exhibits a well-crystallized single phase that can be indexed as tetragonal I4/mmm structure. In the LCNC–LSGM composites patterns, no additional peaks other than LCNC and LSGM are observed, suggesting a good compatibility between LSGM and LCNC.

To understand the influence of Cu on the crystal structure of LCNC, Reitveld refinement are performed on the compositions with $x = 0.0$ and 0.3. For both samples, tetragonal I4/mmm model is considered, as shown in Fig. 2, where La/Ca and O2 are located at 4e (0, 0, z) position, Ni/Cu at 2a (0, 0, 0) and O1 at 4c (0, 0.5, 0) sites. The XRD patterns after final refinement are shown in Fig. 3 and structural parameters obtained based on this model are summarized in Table 1. The results reveal that this model leads to a good fit between the calculated and observed XRD profiles. The substitution

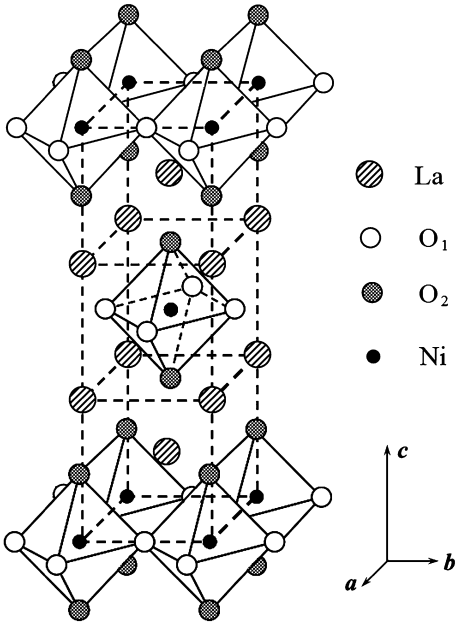

Fig. 2. Tetragonal K_2NiF_4 structure with I4/mmm space group.

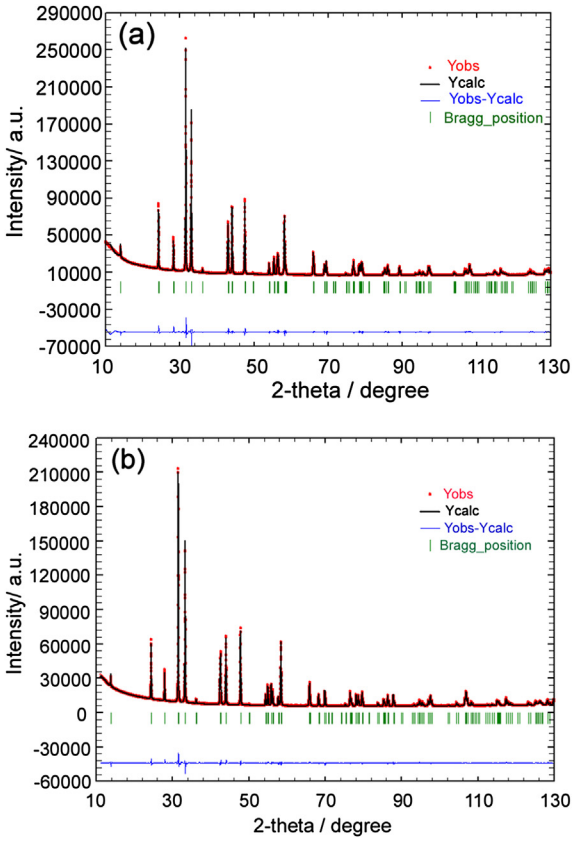

Fig. 3. Observed (points) and calculated (full curve) XRD patterns using I4/mmm model for LCNC with (a) $x = 0.0$ and (b) $x = 0.3$.

of La by Cu results in a decrease in a and b parameters and an increase in c parameter. In details, Cu-doping decreases the Ni(Cu)–O1 or La–O2 (×4) length that determines a and b parameters but increases the Ni(Cu)–O2, La(Ca)–O1 and La(Ca)–O2 (×1) lengths

Table 1
Structural parameters after the Rietveld refinement of XRD data for LCNC.

		$x = 0.0$	$x = 0.3$
$a = b$/Å		3.824(6)	3.802(4)
c/Å		12.594(21)	12.770(21)
V/Å^3		190.554(7)	184.645(4)
La/Ca	z	0.3620(4)	0.3615(2)
	B/Å^2	0.372(17)	0.093(13)
Ni	B/Å^2	0.323(17)	0.284(13)
O1	B/Å^2	0.554(31)	0.215(23)
O2	z	0.1768(29)	0.1786(21)
	B/Å^2	2.070(87)	1.547(65)
R_p/%		7.19	6.66
R_{wp}/%		7.06	6.21
R_{exp}/%		2.25	2.59
χ^2		9.86	5.73
R_b/%		2.28	1.94

Table 2
Interatomic distances (Å) determined from Rietveld refinement of XRD data for LCNC systems.

	$x = 0.0$	$x = 0.3$
La(Ca)–O1 (×4)	2.585(3)	2.596(3)
La(Ca)–O2 (×1)	2.332(4)	2.336(3)
La(Ca)–O2 (×4)	2.748(7)	2.737(5)
Ni(Cu)–O1 (×4)	1.912(1)	1.901(3)
Ni(Cu)–O2 (×2)	2.227(4)	2.281(3)

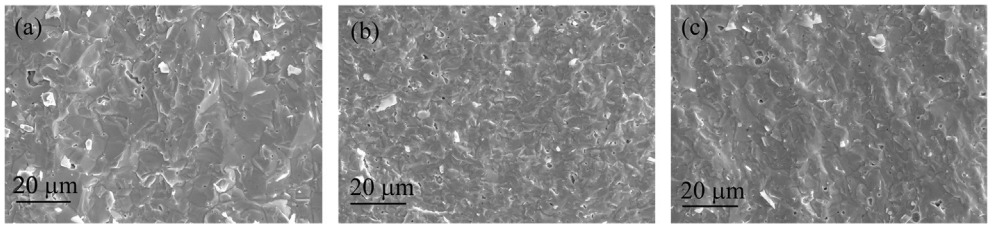

Fig. 4. SEM micrographs of fracture surface of LCNC samples after being sintered at 1200, 1100 and 1000 °C for 6 h for (a) $x = 0.1$, (b) $x = 0.2$ and (c) $x = 0.3$, respectively.

which contribute to the *c* parameter, as listed in Table 2. The variation in bond length can be explained by Jahn–Teller effect encountered in six-coordinate Cu^{2+} complex, where two bonds in the *c*-axis are elongated while the four bonds in *ab* plane are shortened [32]. The overall result is that the cell volume decreases with the content of Cu.

3.2. Sintering behavior

As expected, Cu-doping significantly enhances the sinterability of LCNC. When the Cu content increases from $x = 0$ to $x = 0.3$, the densification temperature of sample decreases from 1350 to 1000 °C for the similar density. For compositions with $x = 0.1$, 0.2

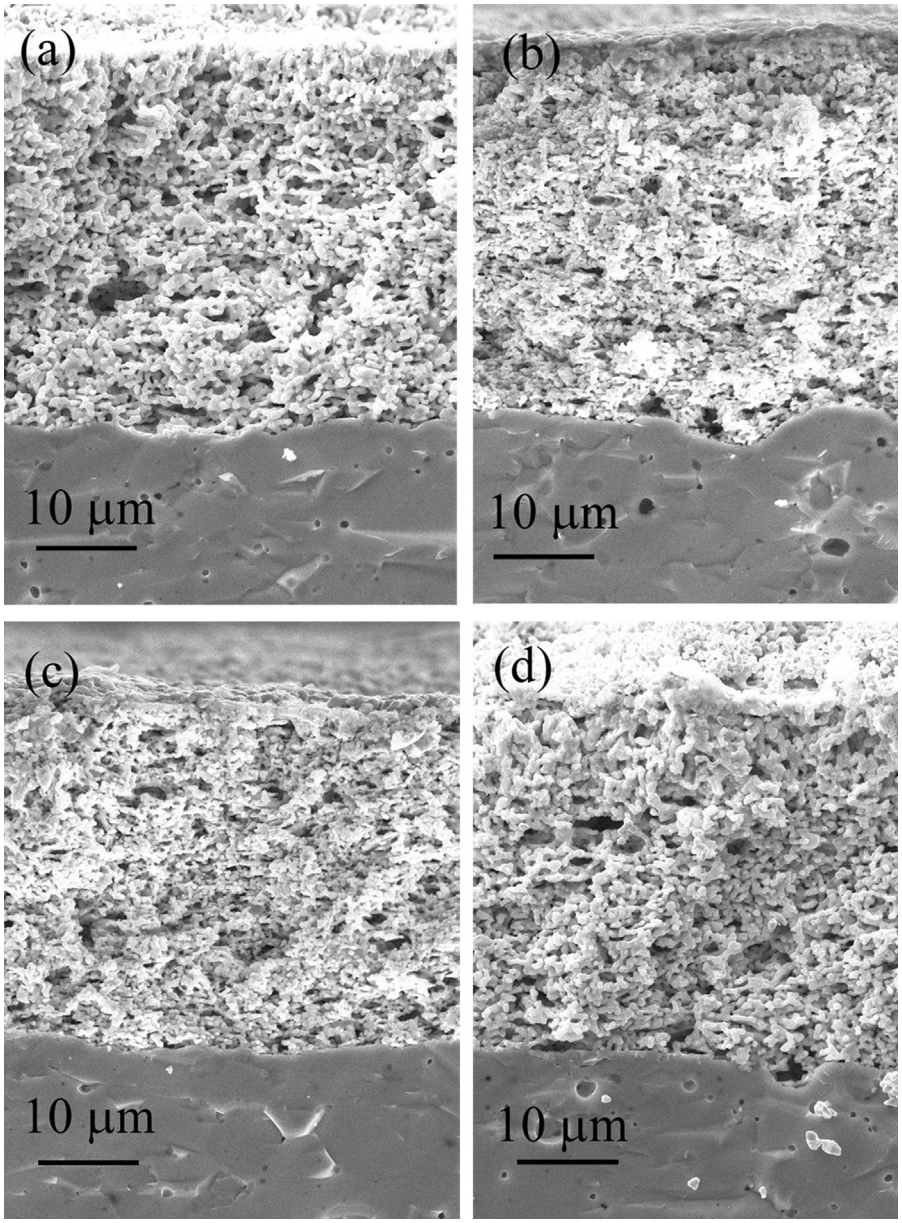

Fig. 5. SEM micrographs of microstructure of LCNC cathode on LSGM electrolyte after being sintered at 950, 900, 900 and 850 °C for 2 h for (a) $x = 0.0$, (b) $x = 0.1$, (c) $x = 0.2$ and (d) $x = 0.3$, respectively.

and 0.3, ceramics with densities about 95% of the theoretic values are achieved after being sintered at 1200, 1100 and 1000 °C for 6 h, respectively (as shown in Fig. 4). Because the electrochemical properties of cathode are much sensitive to its microstructure, the LCNC cathodes with similar porosity are prepared at optimized temperatures of 950, 900, 900 and 850 °C, respectively, for compositions with $x = 0.0$, 0.1, 0.2 and 0.3, as displayed in Fig. 5.

3.3. Electrical conductivity

The temperature dependence of the total electrical conductivity of LCNC samples is shown in Fig. 6(a). Since the ionic conductivity of La_2NiO_4-based materials is usually 10^2–10^4 times less than the electron hole conductivity [10,11], the measured total electrical conductivity of LCNC samples can be regarded as electronic conductivity. The conductivities of all LCNC compositions exhibit the same trends, increasing with temperature through a maximum around 450 °C and then decreasing. The Arrhenius plots of the electrical conductivities show linear relationship, as illustrated in Fig. 6(b), demonstrating the polaron conducting mechanism of these LCNC materials. The electrical conductivity (σ) of semiconductor can be described by Eq. (1).

$$\sigma = \left(\frac{A}{T}\right)\exp\left(\frac{-E_a}{kT}\right) \quad (1)$$

where T stands for the absolute temperature, E_a is the activation energy for electron transportation, A is the pre-exponential factor

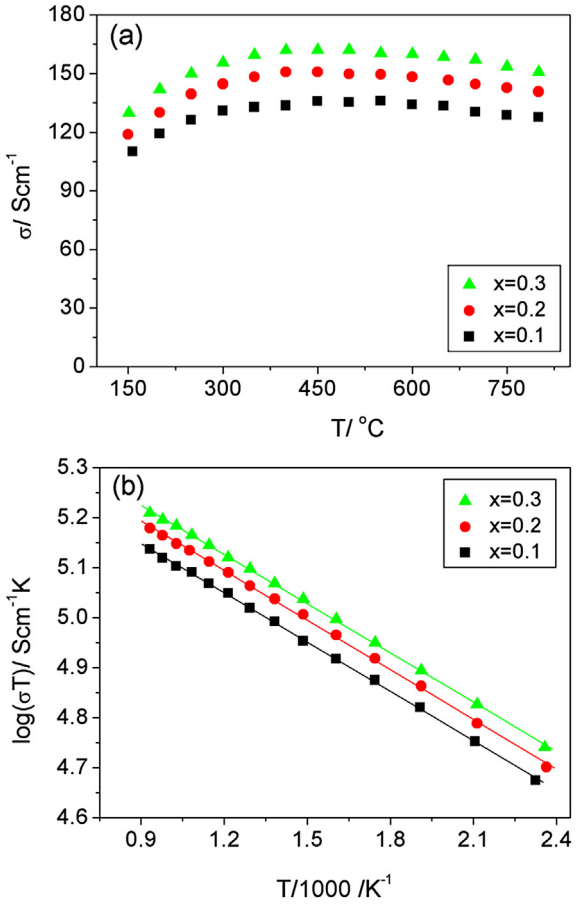

Fig. 6. Electrical conductivity of LCNC as a function of temperature (a) and the Arrhenius plots (b).

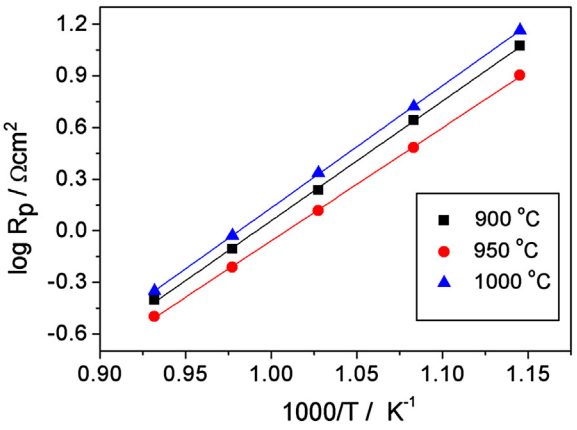

Fig. 7. Effect of sintering temperature on the polarization resistances of $La_{1.7}Ca_{0.3}NiO_{4+\delta}$ electrode.

and k is Boltzmann constant. The temperature has two opposite effects on the conductivity, competing of which leading to a maximum at temperature $T_{max} = E_a/k$.

In isothermal conditions, the conductivities increase obviously with Cu content. Two possibilities contribute to the increase in conductivities with Cu. One possibility is that the substitution of Cu results in a higher interstitial oxygen content due to the elongated c-axis (Table 2), which will increase the density of electron holes for charge compensation. Another possibility correlates to the contraction of Ni(Cu)–O1 equatorial bond lengths (Table 2). As known, the electrical properties are highly anisotropic in $La_2NiO_{4+\delta}$ structure and the carrying of charge mainly takes place in the equatorial planes of NiO_6 octahedron. A shorter Ni(Cu)–O bond length will result in an increase in the covalency of Ni(Cu)–O bond, which may lead to an easy jump and thus a higher mobility of electron holes [20,21,33]. For the sample with $x = 0.3$, the conductivity reaches to 150–160 S cm^{-1} over the range of 600–800 °C.

3.4. Electrochemical properties

The symmetrical cells with configuration of LCNC/LSGM/LCNC are used to measure the AC impedance of LCNC cathodes. Considering that Cu has a remarkable influence on the sintering behavior of $La_{1.7}Ca_{0.3}NiO_4$, the preparation temperature of the electrode may have big impact on the polarization resistance of electrode. The ASR of $La_{1.7}Ca_{0.3}Ni_{1-x}Cu_xO_{4+\delta}$ cathodes after sintered at different temperatures was investigated. As an example, the effect of sintering

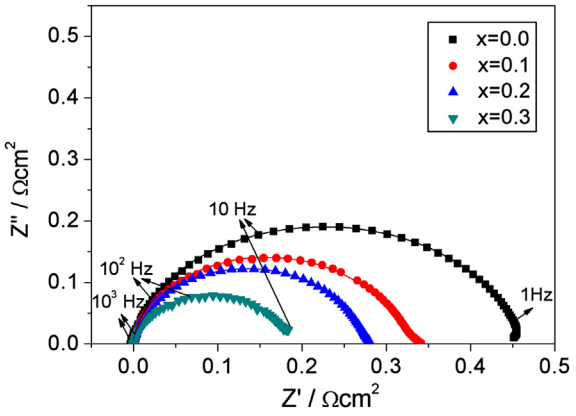

Fig. 8. Impedance spectra of LCNC/LSGM/LCNC symmetrical cells measured at 800 °C.

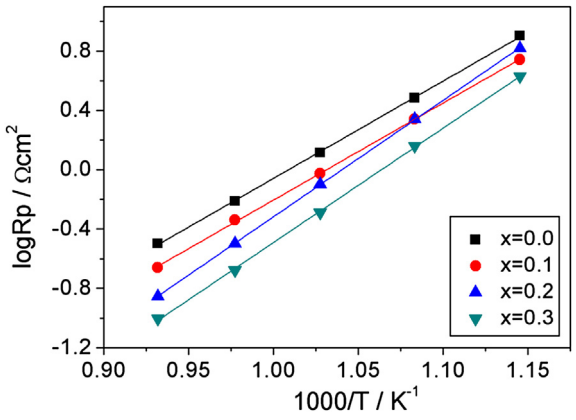

Fig. 9. Temperature dependence of ASR for the cathodes LCNC measured in air.

temperature on the ASR of $La_{1.7}Ca_{0.3}NiO_{4+\delta}$ ($x = 0$) electrode is shown in Fig. 7, where the lowest ASR was achieved by the 950 °C-sintered electrode. High sintering temperature easily results in particle agglomeration and thus low electrode porosity and less specific surface area, which is obviously unfavorable for the electrode reaction, while excessively lower sintering temperature may cause poor contact between particles or between electrode/electrolyte interface, which will lead to large electrode polarization resistance. Similar phenomenon was observed for other composition LCNC cathodes. The optimized sintering temperature for compositions with $x = 0.0$, 0.1, 0.2 and 0.3 is 950, 900, 900 and 850 °C, respectively.

The typical Nyquist plots of these symmetrical cells measured at 800 °C are depicted in Fig. 8. Each spectrum consists of a single depressed arc. In order to make a direct comparison of the polarization resistance of different LCNC cathodes, the ohmic resistances mainly arising form LSGM electrolyte are subtracted from the impedance. Although the arc may consist of two seriously overlapped arcs, the major process should be associated with oxygen atom diffusion and charge transfer steps [6]. The arc decreases significantly with increasing Cu-doping level, demonstrating the reducing polarization resistance. The Arrhenius plots of ASR for LCNC cathodes in air are shown in Fig. 9. Overall, the ASR decreases with increasing Cu content, suggesting Cu-doping has a beneficial effect on the electrode reaction process. The LCNC cathode with $x = 0.3$ gives the lowest polarization resistance that reaches the value of 0.099 Ω cm^2 at 800 °C and 1.45 Ω cm^2 at 650 °C.

In order to make a better understanding of the electrode reaction process, the impedance spectra of electrolyte-supported single cells with configuration of Ni-GDC/LDC/LSGM/LCNC are collected under open circuit voltage (OCV) condition for LCNC cathodes with $x = 0.0$ and 0.3. The results are presented in Fig. 10. Each spectrum consists of a high-frequency induction tail and two well-separated depressed arcs. The former should result from the device and the connect leads while the latter are associated with the electrode process. The equivalent circuit $LR_O(Q_HR_H)(Q_LR_L)$ is used to fit the experiment data, where L is the inductance, R_O is the ohmic resistance of the cell (mainly coming from electrolyte), Q_HR_H and Q_LR_L represent the electrode polarization process in high- (or middle-frequency) and low-frequency region. The corresponding parameters are calculated from the fitting results and inserted in Fig. 10. The characteristic frequencies and capacitances for the high-frequency arcs are 12.6–242.3 Hz and 0.002–0.008 F cm^{-2} for the high-frequency arcs while that for low-frequency arcs are 0.48–

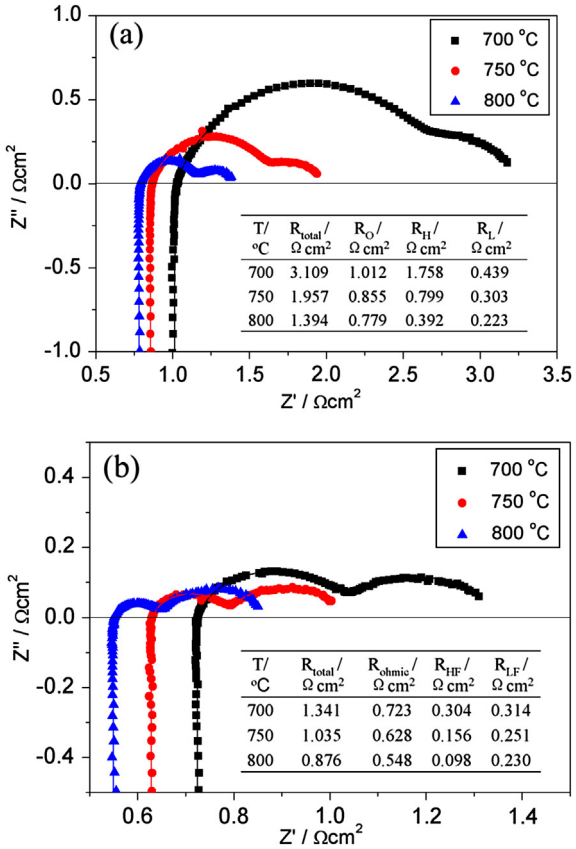

Fig. 10. Impedance spectra of Ni-GDC/LDC/LSGM/LCNC single cells with LCNC (a) $x = 0.0$ and (b) $x = 0.3$ as cathode.

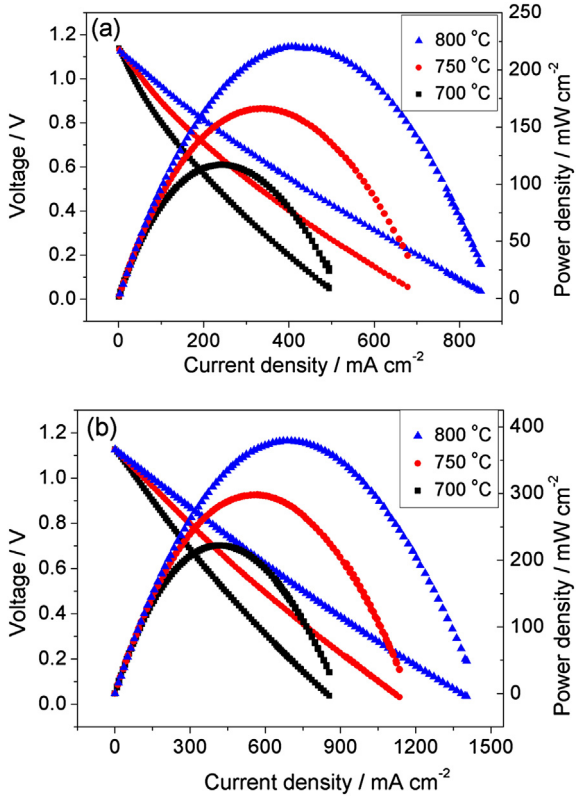

Fig. 11. *I–V* curves of Ni-GDC/LDC/LSGM/LCNC single cells with LCNC (a) $x = 0.0$ and (b) $x = 0.3$ as cathode.

1.36 Hz and 0.04–1.32 F cm^{-2}, indicating the first arc represents the charge transfer process while the second one corresponds to the gas diffusion process [34,35]. With increasing temperature, all the resistances decrease, especially the R_H, indicating that the cell reaction is thermal activation process. To compare the resistance of the two cells, it is clear that the resistance of the cell with $x = 0.3$ is much lower than that with $x = 0.0$, in which the R_H makes the main contribution to the difference. Considering the same anode for the two cells, it can be concluded that the Cu-doping improves remarkably the oxygen transport process of LCNC cathode, which is consistent with the results shown in Fig. 9.

The corresponding I–V curves of the two single cells are plotted in Fig. 11. The cell with $x = 0.3$ has a significantly better performance than that with $x = 0$ and reaches a maximum output power density of 380 mW cm^{-2} at 800 °C. Considering the high resistance mainly coming from the electrolyte (~300 μm), the cell performance is encouraging and much higher power density is expected if thinner LSGM electrolyte is used.

4. Conclusions

The $La_{1.7}Ca_{0.3}Ni_{1-x}Cu_xO_{4+\delta}$ compounds are prepared and investigated as potential cathode materials for intermediate-temperature SOFCs with LSGM as electrolyte. The partial replacement of Cu for Ni has a significant effect on the lattice structure, electrical and electrochemical properties of $La_{1.7}Ca_{0.3}Ni_{1-x}Cu_xO_{4+\delta}$. Cu-doping leads to an elongated Ni(Cu)O_6 octahedron in perovskite layers, corresponding to the decreased a and b but increased c parameters, which causes the increase in electrical conductivity. The substituting Cu also promotes remarkably the sintering process. With the Cu content increasing from $x = 0.0$ to $x = 0.3$, the densification temperature for corresponding ceramics drops from 1350 to 1000 °C and the cathode fabrication temperature reduces from 950 to 850 °C. Cu-doping improves the oxygen transport property and consequently decreases the polarization resistance associated with cathode process, leading to a high cell performance. The maximum output power density reaches 380 mW cm^{-2} at 800 °C for the cell with composition of $x = 0.3$ as cathode. With further modification, such as decreasing the thickness of electrolyte and optimizing the anode structure, much higher power density is expected. The $La_{1.7}Ca_{0.3}Ni_{0.7}Cu_{0.3}O_{4+\delta}$ material is a promising candidate for IT-SOFC cathode.

Acknowledgments

This work was kindly supported by the National Nature Science Foundation of China (No. 20973021) and National Basic Research Program of China (2013CB934003, 2012CB215405).

References

[1] A.J. Jacobson, Chem. Mater. 22 (2010) 660–674.
[2] A. Tarancon, M. Burriel, J. Santiso, S.J. Skinner, J.A. Kilner, J. Mater. Chem. 20 (2010) 3799–3813.
[3] C. Sun, R. Hui, J. Roller, J. Solid State Electrochem. 14 (2010) 1125–1144.
[4] S.B. Adler, Chem. Rev. 104 (2004) 4791–4843.
[5] R. Sayers, M. Rieu, P. Lenormand, F. Ansart, J.A. Kilner, S.J. Skinner, Solid State Ionics 192 (2011) 531–534.
[6] M.J. Escudero, A. Aguadero, J.A. Alonso, L. Daza, J. Electroanal. Chem. 611 (2007) 107–116.
[7] F. Mauvy, C. Lalanne, J.M. Bassat, J.C. Grenier, H. Zhao, L. Huo, P. Stevens, J. Electrochem. Soc. 153 (2006) A1547–A1553.
[8] M.J. Escudero, A. Fuerte, L. Daza, J. Power Sources 196 (2011) 7245–7250.
[9] J. Wan, J.B. Goodenough, J. Zhu, Solid State Ionics 178 (2007) 281–286.
[10] V.V. Kharton, A. Viskup, E.N. Naumovich, F.M.B. Marques, J. Mater. Chem. 9 (1999) 2623–2629.
[11] V.V. Kharton, A.A. Yaremchenko, A.L. Shaula, M.V. Patrakeev, E.N. Naumovich, D.I. Logvinovich, J.R. Frade, F.M.B. Marques, J. Solid State Chem. 177 (2004) 26–37.
[12] V.V. Kharton, A.P. Viskup, A.V. Kovalevsky, E.N. Naumovich, F.M.B. Marques, Solid State Ionics 143 (2001) 337–353.
[13] E. Boehm, J.M. Bassat, P. Dordor, F. Mauvy, J.C. Grenier, P. Stevens, Solid State Ionics 176 (2005) 2717–2725.
[14] S.J. Skinner, J.A. Kilner, Solid State Ionics 135 (2000) 709–712.
[15] M. Greenblatt, Curr. Opin. Solid State Mater. 2 (1997) 174–183.
[16] J. Rodriguez-Carvajal, M.T. Fernandez-Diaz, J.L. Martinez, J. Phys.: Condens. Matter 3 (1991) 3215–3234.
[17] J.B. Goodenough, Rep. Prog. Phys. 67 (2004) 1915–1993.
[18] A. Aguadero, J.A. Alonso, M.J. Martínez-Lope, M.T. Fernández-Díaz, M.J. Escudero, L. Daza, J. Mater. Chem. 16 (2006) 3402–3408.
[19] V.V. Vashook, S.P. Tolochko, I.I. Yushkevich, L.V. Makhnach, L.F. Kononyuk, H. Altenburg, J. Hauck, H. Ullmann, Solid State Ionics 110 (1998) 245–253.
[20] A. Aguadero, M.J. Escudero, M. P′erez, J.A. Alonso, V. Pomjakushin, L. Daza, Dalton Trans. 36 (2006) 4377–4383.
[21] J.P. Tang, R.I. Dass, A. Manthiram, Mater. Res. Bull. 35 (2000) 411–424.
[22] Y. Shen, H. Zhao, X. Liu, N. Xu, Phys. Chem. Chem. Phys. 12 (2010) 15124–15131.
[23] K. Ruck, G. Krabbes, I. Vogel, Mater. Res. Bull. 34 (1999) 1689–1697.
[24] V.V. Vashook, N.E. Trofimenko, H. Ullmann, L.V. Makhnach, Solid State Ionics 131 (2000) 329–336.
[25] H.S. Kim, H.I. Yoo, Solid State Ionics 232 (2013) 129–137.
[26] A. Chroneos, D. Parfitt, J.A. Kilner, R.W. Grimes, J. Mater. Chem. 20 (2009) 266–270.
[27] Q. Li, H. Zhao, L. Huo, L. Sun, X. Cheng, J.C. Grenier, Electrochem. Commun. 9 (2007) 1508–1512.
[28] D. Gostovic, J.R. Smith, D.P. Kundinger, K.S. Jones, E.D. Wachsman, Electrochem. Solid State Lett. 10 (2007) B214–B217.
[29] P.J. Picone, H.P. Jenssen, D.R. Gabbe, J. Cryst. Growth 91 (1988) 463–467.
[30] R. Ruiz-Bustos, A. Cantos-Gómez, A.J. Dossantos-García1, C. Sánchez-Bautista1, J. Duijn, Fuel Cells 11 (2011) 59–64.
[31] E. Boehm, J.M. Bassat, M.C. Steil, P. Dordor, F. Mauvya, J.C. Grenier, Solid State Sci. 5 (2003) 973–981.
[32] A. Aguadero, J.A. Alonso, M.J. Escudero, L. Daza, Solid State Ionics 179 (2008) 393–400.
[33] Z. Li, T. Norby, R. Haugsrud, J. Am. Ceram. Soc. 95 (2012) 2065–2073.
[34] Z. Yang, C. Yang, C. Jin, M. Han, F. Chen, Electrochem. Commun. 13 (2011) 882–885.
[35] J. Peña-Martínez, D. Marrero-López, J. Ruiz-Morales, P. Núñez, C. Sánchez-Bautista, A. Dos Santos-García, J. Canales-Vázquez, Int. J. Hydrogen Energy 34 (2009) 9486–9495.